Fifth-Order Raman Spectroscopy of Excited-State Molecules

Satoru Fujiyoshi,[†,‡,§] Taka-aki Ishibashi,[*,†,‡,⊥] and Hiroshi Onishi[†,‡,§]

Surface Chemistry Laboratory, Kanagawa Academy of Science and Technology (KAST), KSP, Sakado, Takatsu, Kawasaki, 213-0012, Japan, Core Research for Evolutional Science and Technology, Japan Science and Technology Agency, Honmachi, Kawaguchi, 332-0012, Japan, Department of Chemistry, Faculty of Science, Kobe University, Nada, Kobe, 657-8501, Japan, and Department of Chemistry, Graduate School of Science, Hiroshima University, Kagamiyama, Higashi-Hiroshima 739-8526, Japan

Received: August 23, 2004; In Final Form: October 12, 2004

The fifth-order Raman spectroscopy of S_1 *trans*-stilbene in solution was demonstrated. A time domain observation of fifth-order Raman scattering was conducted by using ultrashort, tunable UV and visible pulses. A 22-fs UV pulse at 315 nm induced the first vibrational coherence state of the S_1 state. At the time delays of $t_1 = 0.173$, 0.216, 0.259, and 2.000 ps, a 17-fs visible pulse at 630 nm transferred the first coherence state to the second vibrational coherence state. The time-evolution of the second coherence state was probed by the other 17-fs visible pulse at 630 nm. Thirteen bands due to the fifth-order Raman scattering were identified in the Fourier transformation spectra of the second coherence in the range of 100−1300 cm^{-1}. The intensities and shapes of two bands at 193 and 398 cm^{-1} showed significant t_1 dependence, whereas those of the other 11 bands were insensitive to t_1. The 193-cm^{-1} band was assigned to the depletion of the UV-pump-induced first vibrational coherence (in-plane bending, ν_{25}) by the first visible pulse. Both stepwise creation of the vibrational coherence of the overtone of the ν_{25} mode and the depletion of the first vibrational coherence may have contributed to the 398-cm^{-1} band. The 11 other bands are equivalents of time-resolved spontaneous Raman bands (third-order optical process) of S_1 *trans*-stilbene.

1. Introduction

Redistribution of vibrational energy deposited by photoexcitation to other vibrational modes plays important roles in photochemical reactions, such as isomerization and bond dissociation. Combination (or overtone) vibrational modes in excited states act as such energy-accepting modes. Probing the vibrational bandwidths, shapes, and frequencies of these modes is important to understanding of the vibrational energy redistribution. Their bandwidths and shapes reflect dephasing dynamics of the accepting modes. The frequencies provide information on unharmonicities of the multidimensional potential surface that determine the coupling between the initially excited Franck−Condon modes and other vibrational coordinates. However, the investigation of the combination modes is difficult with linear spectroscopies, such as time-resolved Raman and infrared spectroscopies. Although some combination bands are sometimes observed, the distinctions between these bands and fundamental vibrational bands are difficult with these spectroscopies.

It was theoretically proposed that fifth-order Raman spectroscopy provides more information on the combination modes than linear spectroscopies do.[1,2] Experimental investigations have demonstrated the ability of this method to probe vibrational mode couplings and dynamics of the combination bands.[3−8] However, two cascading third-order optical processes were sometimes misidentified as a fifth-order process.[9−11] Although the experimental difficulties have been partially fixed by using a heterodyne detection and a unique phase-matching geometry, the application of the technique was limited to ground-state molecules with high nonlinearity such as carbon disulfide in the electronic nonresonance condition.[12,13] Fifth-order Raman spectroscopy has a potential for probing combination modes in an electronic excited state. In the present paper, fifth-order Raman measurements of excited-state molecules are demonstrated. The fifth-order Raman signal of S_1 *trans*-stilbene was enhanced with tunable, ultrashort UV and visible pulses the wavelengths of which are in resonance with the $S_n \leftarrow S_1$ and $S_1 \leftarrow S_0$ transitions of *trans*-stilbene.

2. Optical Transitions of Interest

Figure 1a shows a diagram of fifth-order Raman spectroscopy of excited-state molecules. A UV-pump pulse having a 22-fs duration excites *trans*-stilbene to the S_1 state of $|g\rangle\langle g|$ and $|f_1\rangle\langle f_1|$, as well as to the vibrational coherent states of $|g\rangle\langle f_1|$ and $|f_1\rangle\langle g|$ because the bandwidth of the UV-pump pulse is more than 650 cm^{-1}.[14−16] g is the vibrational ground state of the S_1 state, and f_1 is the S_1 vibronic state having a Franck−Condon overlap with the vibrational wave functions of the S_0 state.[14] We used two visible (P_{1-2} and P_3) pulses with a 17-fs duration and a 900-cm^{-1} bandwidth. At a time delay of t_1, the broadband P_{1-2} pulse transferred the first coherence states of $|g\rangle\langle f_1|$ and $|f_1\rangle\langle g|$ to the second coherence states of $|g\rangle\langle f_2|$ and $|f_2\rangle\langle g|$ via a Raman pumping process ($f_1 \rightarrow S_n \rightarrow f_2$). f_2 denotes another S_1 vibronic state. If f_2 is the vibrational combination state of the S_1 state, information about the combination state can be obtained by this method. The second interaction by the P_{1-2} pulse induces an additional absorbance change that is probed by the P_3 pulse. The interval between the P_{1-2} and P_3 pulses is t_2. The whole

* To whom correspondence should be addressed. E-mail: taib@hiroshima-u.ac.jp.
† Kanagawa Academy of Science and Technology (KAST).
‡ Japan Science and Technology Agency.
§ Kobe University.
⊥ Hiroshima University.

10.1021/jp0461899 CCC: $27.50
Published on Web 12/01/2004

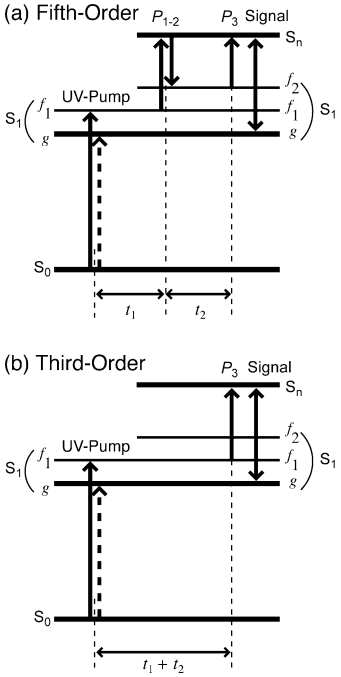

Figure 1. Energy diagrams of the fifth-order (a) and third-order (b) Raman processes of excited-state molecules: g, the vibrational ground state on the S_1 state; t_1, the time delay between the UV-pump and P_{1-2} pulses; t_2, the time-delay between the P_{1-2} and P_3 pulses; f_1, the S_1 vibronic states having a Franck−Condon overlap with the S_0 state; f_2, the other S_1 vibronic states. The solid and dashed arrows represent a ket- and a bra-side transition, respectively, between the connected levels.

process contains five incident electric fields, and thus the signal field, E_{fifth}, is proportional to the fifth-order optical response, $\chi^{(5)}(t)$. The spectral sensitivity curve of the present measurements depends on the convolution function of the UV-pump, P_{1-2}, and P_3 intensities, Gaussian functions having full width at half-maxima (fwhm) of 22, 17, and 17 fs, respectively. That convolution function in the present work was given by a Gaussian function having a fwhm of 33 fs. The sensitivity curve calculated by the Fourier transformation (FT) analysis of the convolution function was a Gaussian function centered at 0 cm^{-1} having a half-width at half-maximum (hwhm) of ca. 450 cm^{-1}. On the other hand, when the time delay t_1 is sufficiently longer than the dephasing time (T_v) of the vibrational coherence generated by the UV-pump pulse, the obtained signal is equivalent to the third-order optical response, $\chi^{(3)}(t)$, of the excited-state molecules.[17−20] The spectral sensitivity curve of this response depends on the P_{1-2} pulse and on the P_3 pulse and not on the UV-pump pulse. This is because the amplitude of $|g\rangle\langle g|$ or $|f_1\rangle\langle f_1|$ at the arrival time of the P_{1-2} pulse is independent of the UV-pulse width. Therefore, the sensitivity curve can be calculated by the FT analysis of the convolution function of the P_{1-2} intensity with the P_3 intensity, and it was given by a Gaussian function centered at 0 cm^{-1} having a hwhm of ca. 600 cm^{-1}.

The wavelength of the P_{1-2} and P_3 pulses is tuned to the electronic absorption of the S_1 molecules to obtain the resonance enhancement. The resonance enhancement provides two advantages to the fifth-order spectroscopy. (1) Owing to the resonance enhancement, the P_{1-2} pulse can dominantly excite the S_1 molecules generated by the UV-pump pulse, and the doubly photoexcited molecules are probed by the P_3 pulse. Thus, the fifth-order Raman response of S_1 *trans*-stilbene can be selectively detected. (2) The final interaction of the fifth-order Raman process ($f_2 \rightarrow S_n \rightarrow g$) is regarded as an equivalent of

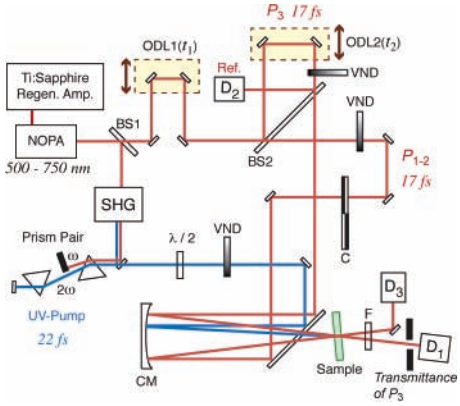

Figure 2. Apparatus used for the fifth-order Raman measurements: NOPA, noncollinear optical parametric amplifier; BS, beam splitters; ODL, optical delay lines; SHG, a crystal for the second harmonic generation; VND, variable neutral density filters; C, synchronous mechanical chopper; CM, concave mirror; F, filter for the rejection of the pump pulse and the fluorescence of the sample; D, photodiodes.

the resonance anti-Stokes Raman process of the combination modes when f_2 is a combination mode. The transition probability of this final interaction is proportional to the Raman cross section of the combination transitions. The probability can be enhanced in a resonance condition because the cross section of the combination transition relative to those of fundamental transitions in a resonance condition is much larger than that in a nonresonance condition. The first and second coherence states are time-evolved on the S_1 state in our scheme. Thus we call the present method "fifth-order Raman spectroscopy of excited-state molecules" although the initial state is the S_0 state.

3. Experimental Setup

The apparatus used for the fifth-order Raman measurements is shown in Figure 2. The light source was a noncollinear optical parametric amplifier (NOPA, TOPAS-*white*, Quantronix) pumped by a Ti:sapphire regenerative amplifier (Hurricane, Spectra Physics) operated at 1 kHz. The wavelength of the output was tunable in the range of 500−750 nm. The visible output (630 nm) was divided into four parts for the UV-pump, P_{1-2}, P_3, and reference pulses. The UV-pump pulse was generated by the second harmonic generation of the output of the NOPA with a 50-μm-thick β-BaB_2O_4. The generated UV-pulse (315 nm) was passed through fused-silica prism pairs (with an apex−apex distance of 210 mm) for the group-velocity-dispersion compensation.[14] The UV-pump, P_{1-2}, and P_3 pulses were spatially crossed at a sample jet. Polarizations of all the pulses were parallel. The UV-pump, P_{1-2}, and P_3 energies were 0.15, 0.07, and 0.02 μJ, respectively, and their spot diameters at the sample position were ~0.1 mm. The intensities of the P_3 and reference pulses were detected by photodiodes (S1226-18BU, Hamamatsu) coupled with current preamplifiers (LI-76, NF Corporation), and the difference of the photodiode outputs was amplified with a differential amplifier (5307, NF Corporation). The differentially amplified output was gated with a boxcar integrator (SR250, Stanford Research Systems), A/D converted, and sent to a personal computer on a pulse-to-pulse basis. The P_{1-2} pulse was modulated at 500 Hz with a synchronous mechanical chopper (3501, New Focus). The signals with P_{1-2} on and off were separately accumulated on the computer, and the P_{1-2}-induced absorbance change was calculated. The instrumental response and the time origins of t_1 and t_2 at the sample position were determined using the intensity cross-correlation with a 50-μm-thick β-BaB_2O_4 crystal. The fwhm of

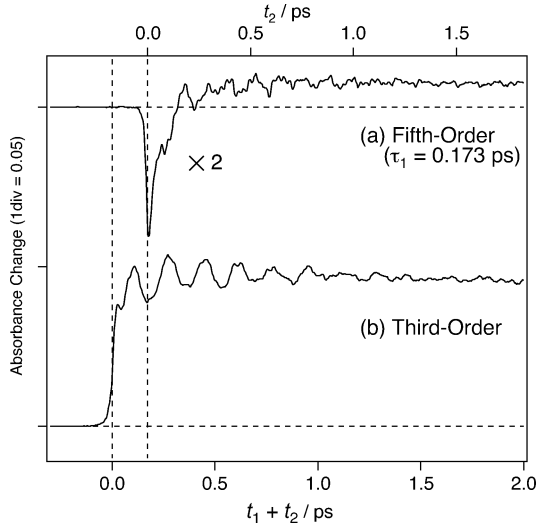

Figure 3. (a) Time-resolved fifth-order Raman signal of S_1 *trans*-stilbene in hexadecane solution at $t_1 = 0.173$ ps (UV-pump, 315 nm; P_{1-2} and P_3, 630 nm). The vertical axis is expanded by a factor of 2. (b) Time-resolved absorption signal of S_1 *trans*-stilbene in hexadecane. The interval of data points was 4 fs in both figures. Each data point was obtained by averaging over 2000 (a) and 4600 (b) probe pulses.

the cross correlation between the UV-pump and P_3 pulses was 28 fs, and that between the P_{1-2} and P_3 pulses was 24 fs. The intensity time widths (fwhm) of the 315-nm and 630-nm pulses were estimated to be 22 and 17 fs on the assumption that the pulse shapes were Gaussian functions. *trans*-Stilbene (Tokyo Kasei) was dissolved in hexadecane (99+%, Aldrich) at the concentration of 10 mmol/L. A thin-film jet of the solution was used as the sample. The efficient thickness was estimated to be ca. 50 μm from the penetration depth of the pump pulse although the thickness of the sample jet was >300 μm. We set the efficient thickness to be thin to avoid the group velocity dispersion of the light pulses in the solution.[21]

4. Results

In the fifth-order Raman measurements, the UV-pump pulse at 315 nm was used to populate S_1 *trans*-stilbene, and the wavelength of the visible P_{1-2} and P_3 pulses was set at 630 nm to be resonant with the absorption band of S_1 *trans*-stilbene.[22] The time-resolved absorbance change of S_1 *trans*-stilbene induced by the P_{1-2} pulse as a function of t_2 was measured with the P_3 pulse (Figure 3a). The time delay t_1 was set to be 0.173 ps. The signal was composed of a oscillatory modulation, a sharp peak around the time origin of t_2, and a nonoscillatory background. The oscillatory modulation is due to the second coherence state of S_1 *trans*-stilbene and is the fifth-order Raman signal. The sharp peak and the nonoscillatory background were well-fitted with a sum of three exponential functions convoluted with the correlation function of the P_{1-2} and P_3 pulses (a Gaussian function having an fwhm of 24 fs) in the range of -0.3 to 3 ps. Time constants of $\tau_1 < 24$ fs, $\tau_2 = 0.10$ ps, and $\tau_3 > 3$ ps and amplitudes of $A_1 = -0.012$, $A_2 = -0.020$, and $A_3 = 0.004$ were evaluated. The τ_1 and τ_2 components were interpreted as the resonance electronic response of S_1 *trans*-stilbene and its population recovery process due to an $S_n \rightarrow S_1$ internal conversion, respectively.[18] The τ_3 component was assigned to both the vibrational cooling of the S_1 state and the population recovery of S_0 *trans*-stilbene.[18,23]

To investigate what vibrational modes were induced by the UV-pump pulse, we carried out a similar time-resolved absorption measurement without the P_{1-2} pulse. Figure 3b shows time-resolved absorption of *trans*-stilbene measured with the same wavelengths and pulse energies of the UV-pump and P_3 pulses as in Figure 3a. The UV-pump pulse instead of the P_{1-2} pulse was modulated at 500 Hz with the synchronous mechanical chopper. An absorbance change induced by the UV-pump pulse was probed by the P_3 pulses. The measurement corresponds to the third-order pump−probe experiment shown in Figure 1b. The absorption signal was composed of a periodic modulation due to a vibrational coherence of S_1 *trans*-stilbene superimposed on the $S_n \leftarrow S_1$ electronic transition. The present signal reproduced the previous result reported by Takeuchi and Tahara.[14] The large periodic modulation at the period of 0.19 ps was assigned to the Raman-active vibrational mode of S_1 *trans*-stilbene (200 cm^{-1}, in-plane bending, ν_{25}).[14] It decayed exponentially with a time constant of 0.5 ps. We confirmed that the vibrational coherence of the ν_{25} mode was mainly created by the UV-pump pulse. The time t_1 of 0.173 ps in Figure 3a corresponds to the phase shift of the ν_{25} mode ($\theta_{25} = 2\pi\nu_{25}t_1$) of 2.0π. The nonoscillatory components were well-fitted with a sum of two exponential functions convoluted with the cross-correlation function of the pump and P_3 (a Gaussian function having an fwhm of 28 fs). Time constants of $\tau_1 = 0.11$ ps and $\tau_2 > 3$ ps and amplitudes of $A_1 = -0.012$ and $A_2 = 0.048$ were evaluated.

We carried out the fifth-order Raman measurements at $t_1 = 0.216$, 0.259, and 2.000 ps with the same experimental conditions of Figure 3a. The three t_1 delays correspond to the phase shift θ_{25} of 2.5π, 3.0π, and 11.6π. The nonoscillatory components of the fifth-order Raman signals at the three time delays were similar to that at $t_1 = 0.173$ ps (Figure 3a) and fitted with a sum of three exponential functions.

To extract the oscillatory components, the nonoscillatory components were subtracted from the total signals by the fitting analysis. The oscillatory components as a function of t_2 were Fourier transformed to frequency-domain spectra. To smooth the transformed spectra, the subtracted oscillations at 0−3 ps were multiplied by a window function (a Gaussian function having an fwhm of 3 ps centered at $t_2 = 0$ ps), and zero data points were added at 3−30 ps before the FT analysis. Figure 4a−d shows the real parts of the FT spectra, and Figure 4f−i shows their imaginary parts at the four time delays of t_1. The oscillatory component as a function of $t_1 + t_2$ of the third-order signal in Figure 3b was also extracted and Fourier transformed to the vibrational spectra in the same manner. The real and imaginary parts of the FT spectra of the third-order signal are shown in Figure 4e,j. The ν_{25} band (193 cm^{-1}) was dominantly observed, while it was very small in the fifth-order spectrum with $t_1 = 2.000$ ps (Figure 4d).

In the fifth-order FT spectra, 13 vibrational bands were identified at 1234, 1174, 1143, 1072, 978, 848, 781, 721, 615, 461, 398, 287, and 193 cm^{-1}. These bands can be classified into two groups, the bands that showed significant t_1 dependence (398 and 193 cm^{-1} bands) and the other 11 bands that were insensitive to t_1. The bands in the latter group correspond to spontaneous Raman bands of S_1 *trans*-stilbene. As seen in Figure 3b, the vibrational coherence induced by the UV-pump pulses almost faded away at t_1 of 2.000 ps. Thus, the FT spectra with $t_1 = 2.000$ ps (Figure 4d,i) should be similar to the third-order Raman spectrum of S_1 *trans*-stilbene. Eleven bands in the range of 1234−287 cm^{-1} were observed by time-resolved spontaneous Raman measurements, eight bands were assigned to a_g modes of the S_1 state (ν_{14}, ν_{16}, ν_{17}, ν_{18}, ν_{20}, ν_{21}, ν_{22}, and ν_{24}).[24−27] The vibrational bands in the real part had negative, symmetric shapes,

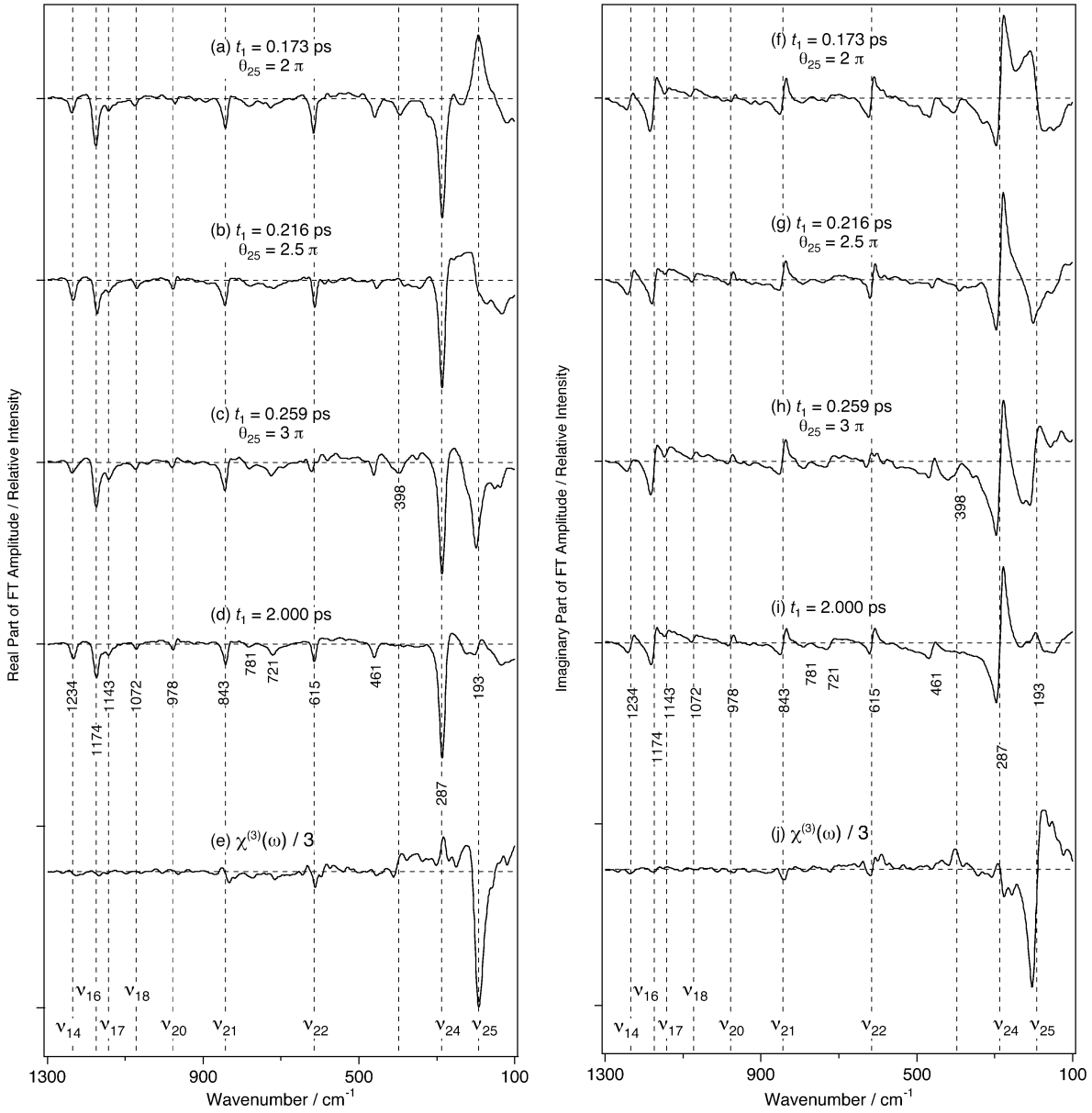

Figure 4. The real part of the FT spectra of the fifth-order Raman signal at t_1 = (a) 0.173, (b) 0.216, (c) 0.259, and (d) 2.000 ps and the imaginary part of the FT spectra at t_1 of (f) 0.173, (g) 0.216, (h) 0.259, and (i) 2.000 ps. The delay times t_1 correspond to the phase shift θ_{25} of (a,f) 2.0π, (b,g) 2.5π, (c,h) 3.0π, and (d,i) 11.6π. The (e) real and (j) imaginary parts of the FT spectra of the beat components of the third-order time-resolved absorption signals are also shown. The vertical axes of (e) and (j) are reduced by a factor of 3.

and those in the imaginary part had dispersive shapes. Therefore, the vibrational coherence at t_1 of 2.000 ps can be expressed as

$$\Delta A_{\text{fifth}}(t_2) \propto \sum_{\nu} A_{\nu} \cos[2\pi\nu_{\nu}t_2 + \varphi_{\nu}(t_1)] \exp(-t_2/T_{\nu}) \quad (1)$$

with $\varphi_{\nu}(t_1 = 2.000 \text{ ps}) \approx \pi$, where A_{ν}, ω_{ν}, φ_{ν}, and T_{ν} are the amplitude, frequency, initial phase, and dephasing time of each vibrational mode. In time-domain resonance Raman measurements due to $\chi^{(3)}$, the phases, φ_{ν}, are often close to either 0 or π, so the vibrational bands in the real part of the FT spectrum have symmetric shapes, whereas in the imaginary part, they have dispersive shapes.[28−31] The band characteristic of the present observation at t_1 of 2.000 ps (Figure 4d,i) is consistent with that of the time-domain Raman measurements in the resonance condition.[32]

The intensities and band shapes of the 398 and 193 cm^{-1} bands largely depended on t_1. The frequency of the 193-cm^{-1} band agreed with that of the ν_{25} mode observed in the third-order pump−probe measurements (Figure 4e). In contrast, the intensity of the 398-cm^{-1} band was very small both in the third-order signal (Figure 4e) and in the fifth-order signal at 2.000 ps (Figure 4d). The temporal behavior of these bands suggests that they are unique for the fifth-order response. We discuss the origin of the bands in section 5.

To confirm that the fifth-order Raman signal originated from S_1 *trans*-stilbene, we measured the P_{1-2} pulse induced absorbance changes with and without the UV-pump pulse under the same conditions of Figure 3a. The signal without the pump pulse (Figure 5a) consisted of only the sharp peak assigned to the nonresonance electronic response of the ground-state molecules.[18,33] The signal due to the vibrational coherence of the ground-state molecules (Figure 5a) was negligible compared with that of the fifth-order Raman signal (Figure 5b). This confirmed that the observed oscillatory components by the fifth-

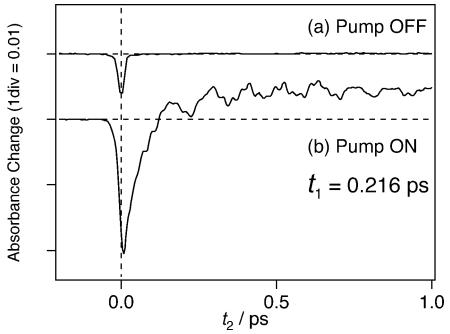

Figure 5. P_{1-2} pulse induced absorbance change of trans-stilbene (a) measured without the UV-pump pulse or (b) measured with the UV-pump pulse (the fifth-order Raman signal).

order Raman signal (Figure 3a) have no contributions from the signal of the ground-state molecules created by the P_{1-2} and P_3 pulses.

In studies of ground-state molecules, it is often difficult to distinguish a fifth-order process from a cascading third-order process.[9−11] The cascading process generates a signal in the same phase matched direction and with the same dependence on the laser fluence. For example, a signal due to the first third-order process can act as a probe light for the second third-order process, a so-called parallel cascading third-order process.[10,11] In our experiment, the third-order signal, $E_s^{(3)}$, of ground-state molecules generated by P_{1-2} and P_3 pulses possibly serves as the P_3 light in the third-order process of S_1 *trans*-stilbene (Figure 1b). The cascading process induced by the electric fields of the UV-pump and $E_s^{(3)}$ may be misidentified as a fifth-order Raman signal, because the phase matching conditions and laser fluence dependence of the cascading signal are the same as those of the fifth-order Raman signal. However, we expect that this type of cascading process did not contribute to the signal. This is because $E_s^{(3)}$ was negligibly small due to the off-resonant condition of the P_{1-2} and P_3 pulses for the ground-state molecules (see Figure 5a).

5. Discussion

The fifth-order Raman spectra in Figure 4 contained the 13 bands in the range of 100−1300 cm^{-1}. The band characteristics of the two bands at 193 and 398 cm^{-1} were sensitive to t_1. We discuss the origin of these bands in sections 5-1 and 5-2 and then the equivalence of the other 11 bands to the time-resolved spontaneous Raman bands in section 5-3.

5-1. Depletion of Vibrational Coherence (ν_{25}, 193 cm^{-1}). The band shape of the 193-cm^{-1} band (ν_{25}) largely depended on t_1 (Figure 4a−c). At $t_1 = 0.173$ ps ($\theta_{25} = 2.0\pi$), the band had a positive, symmetric shape in the real part. The band characteristic shows that the phase of the vibrational coherence φ_v is $2n\pi$ ($n = 0, 1, ...$) in eq 1. In contrast, the band at $t_1 = 0.216$ ps ($\theta_{25} = 2.5\pi$) had a dispersive shape in the real part, whereas it had a negative, symmetric shape in the imaginary part. The shapes of the band indicate that the phase φ_v is $(2n + 0.5)\pi$. Also, the band shape at $t_1 = 0.259$ ps and $\theta_{25} = 3.0\pi$, (Figure 4c,h) indicates that the phase φ_v is $(2n + 1)\pi$. The results show that the phase of the band synchronized with the phase shift θ_{25}.

The phase dependence of the 193-cm^{-1} band can be explained by the depletion process of the first vibrational coherence. As seen in the third-order spectra (Figures 4e,j), the vibrational coherence of the ν_{25} mode was mainly generated by the UV-pump pulse at $t_1 = 0$ ps. Therefore, the oscillatory component

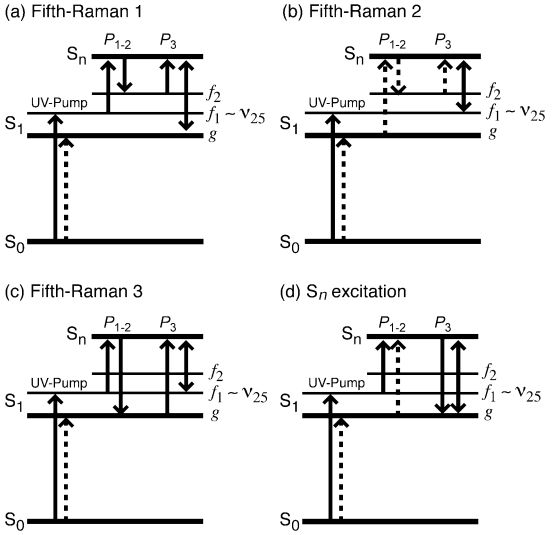

Figure 6. Energy diagrams of possible depletion processes of the ν_{25} mode: f_2 is fundamental, overtone, or combination states of S_1 *trans*-stilbene.

of the UV-pump-induced absorbance change can be approximated as

$$\Delta A_{pump}(t_1,t_2) \approx A_{25}^0 \cos[2\pi\nu_{25}(t_1 + t_2) + \pi] \exp[-(t_1 + t_2)/T_{25}]$$
$$\approx -A_{25}^0 \cos[2\pi\nu_{25}(t_1 + t_2)] \exp[-(t_1 + t_2)/T_{25}] \quad (2)$$

If the coherence is bleached by the second P_{1-2} pulse, the depletion signal for the oscillatory part is given by

$$\Delta A_{depletion}(t_1,t_2) = -N\Delta A_{pump}(t_1,t_2)$$
$$\approx A(t_1) \cos[2\pi\nu_{25}t_2 + \theta_{25}(t_1)] \exp[-t_2/T_{25}] \quad (3)$$

where $A(t_1) = NA_{25}^0 \exp[-t_1/T_{25}]$, $\theta_{25}(t_1) = 2\pi\nu_{25}t_1$, and N denotes the probability of the depletion process. Equation 3 shows that the center frequency is constant (ν_{25}), and the phase, $\theta_{25}(t_1)$, is modulated by the frequency of ν_{25} (193 cm^{-1}) as a function of t_1. The predicted $\theta_{25}(t_1)$ agrees with the t_1 dependence of the 193-cm^{-1} band in the fifth-order Raman spectra. Therefore, we assign the 193-cm^{-1} band to the P_{1-2} induced depletion of the first vibrational coherence (ν_{25}).

Possible depletion processes of the ν_{25} mode are shown in Figure 6. First, we consider three fifth-order Raman processes in Figure 6a−c. The fifth-order Raman 1 process transfers the vibrational coherence of the ν_{25} mode to that of the other vibrational modes (f_2). As in the fifth-order Raman 1 process, the processes of the fifth-order Raman 2 and 3 transfer the vibrational coherence of the ν_{25} mode to the vibrational coherence at the frequency of $\nu_{25} - \nu_{f_2}$ and the vibrational ground state, respectively. Second, the S_n excitation also causes the depletion of the vibrational coherence of the ν_{25} mode (Figure 6d). The P_{1-2} pulse can excite the S_1 molecules to the S_n state. Although a vibrational coherence in the S_n state can be generated by the P_{1-2} pulse, the coherence may vanish within <100 fs by an $S_n \rightarrow S_1$ internal conversion as well as the other relaxation processes of a direct $S_n \rightarrow S_0$ transition.[18,34]

5-2. Fifth-Order Raman Band at 398 cm^{-1}. Here we consider three possible interpretations of the origin of the 398-cm^{-1} band: the band originates from (1) a fundamental vibrational band of the S_n state, (2) the P_{1-2}-induced depletion of the coherence generated by the UV-pump pulse as in the

case of the 193 cm^{-1} band, or (3) the first overtone of the ν_{25} mode ($2\nu_{25}$) of S_1 *trans*-stilbene excited stepwise by the UV-pump and P_{1-2} pulses ($|S_0\rangle\langle S_0| \rightarrow |g\rangle\langle \nu_{25}| \rightarrow |g\rangle\langle 2\nu_{25}|$ and $|S_0\rangle\langle S_0| \rightarrow |\nu_{25}\rangle\langle g| \rightarrow |2\nu_{25}\rangle\langle g|$ in Figure 1a). For the first case, the observed bandwidth of the 398 cm^{-1} band ($\sim$40 cm^{-1}) was much smaller than that (100 cm^{-1}) expected for the bands of the S_n state with the lifetime of 0.1 ps. We thus rule out the first interpretation. Next, the second possibility is examined. Small bands were observed in the FT spectra of the third-order pump−probe signal (Figure 4e,j). This indicates that vibrational coherence having a frequency of $\sim$400 cm^{-1} was induced by the UV-pump process. Thus, the depletion process of the vibrational coherence at $\sim$400 cm^{-1} may have contributed to the 398-cm^{-1} band. In this case, the phase of this depletion process, $\varphi_\nu(t_1)$, should have synchronized its own frequency ($\sim$400 cm^{-1}) as a function of t_1 as in the case of the 198 cm^{-1} band. For the third case, the frequency of the 398-cm^{-1} band was identical with that of the first overtone of the ν_{25} mode (398 cm^{-1}) measured by a supersonic beam technique.[25] The fact that the frequency of the ν_{25} mode measured by the supersonic beam[25] is in excellent agreement with that in the solution[24] supports that the overtone frequency in the beam might be close to that in solution. Thus, the first overtone of S_1 *trans*-stilbene excited stepwise by the UV-pump and P_{1-2} pulses may also have contributed to the 398-cm^{-1} band. The phase shift of the coherence as a function of t_1, $\varphi_\nu(t_1)$, should synchronize with the frequencies of $|g\rangle\langle \nu_{25}|$ and $|\nu_{25}\rangle\langle g|$ (193 cm^{-1}).

As seen in the FT spectra (Figure 4), the amplitude of the 398-cm^{-1} band was nearly zero in both the real and imaginary parts of FT spectra at $t_1 = 0.216$ ps (Figure 4b,g) although the band appeared at $t_1 = 0.173$ and 0.259 ps. This temporal behavior can be attributed to an interference between more than two bands having different t_1 dependences. Thus, the depletion process the phase of which synchronizes at $\sim$400 cm^{-1} and the fifth-order Raman process of the first overtone of the ν_{25} band the phase of which synchronizes at 193 cm^{-1} may have contributed to the 398-cm^{-1} band. Further experiments involving the fine scans of t_1 or the 2D spectra of the fifth-order Raman signal may provide the t_1 dependence of the 398-cm^{-1} band, such as its modulation frequencies and its phase as the function of t_1, leading to a conclusive assignment.

5-3. Possible Contribution of Signals in our Setup. We discuss possible contribution of signals in the fifth-order Raman setup. We define the wave vectors of the UV-pump, P_{1-2}, and P_3 pulses as $\mathbf{k}_{\text{pump}}$, $\mathbf{k}_{1-2}$, and $\mathbf{k}_3$, respectively. The observed signal fields had the wave vector of $\mathbf{k}_3$ because the transmittance changes of the P_3 pulse were detected in the present study. The signals due to the fifth-order process as well as the third-order processes are irradiated to the direction having the wave vector of $\mathbf{k}_3$. First, we consider the fifth-order Raman signal having a wave vector of $\mathbf{k}_{\text{pump}} - \mathbf{k}_{\text{pump}} + \mathbf{k}_{1-2} - \mathbf{k}_{1-2} + \mathbf{k}_3$, induced by all the optical pulses. This signal contains the fifth-order Raman signal of the S_1 *trans*-stilbene ($E_{\text{fifth}-S_1}$ in Figure 7a) and the ground-state molecules ($E_{\text{fifth}-S_0}$ in Figure 7b,c). Second, the third-order processes are induced by only the UV-pump and P_3 pulses. The wave vector is $\mathbf{k}_{\text{pump}} - \mathbf{k}_{\text{pump}} + \mathbf{k}_3$. The signal is contributed from the pump−probe processes of S_1 *trans*-stilbene ($E_{\text{pump}-\text{probe}-S_1}$ in Figure 7d) and the ground-state molecules ($E_{\text{pump}-\text{probe}-S_0}$ in Figure 7e,f). Third, the other third-order processes having a wave vector of $\mathbf{k}_{1-2} - \mathbf{k}_{1-2} + \mathbf{k}_3$ can be detected by the present setup. The process is attributed to the third-order Raman signal of the ground-state molecules probed by the P_{1-2} and P_3 pulses ($E_{\text{third}-S_0}$ in Figure 7g).

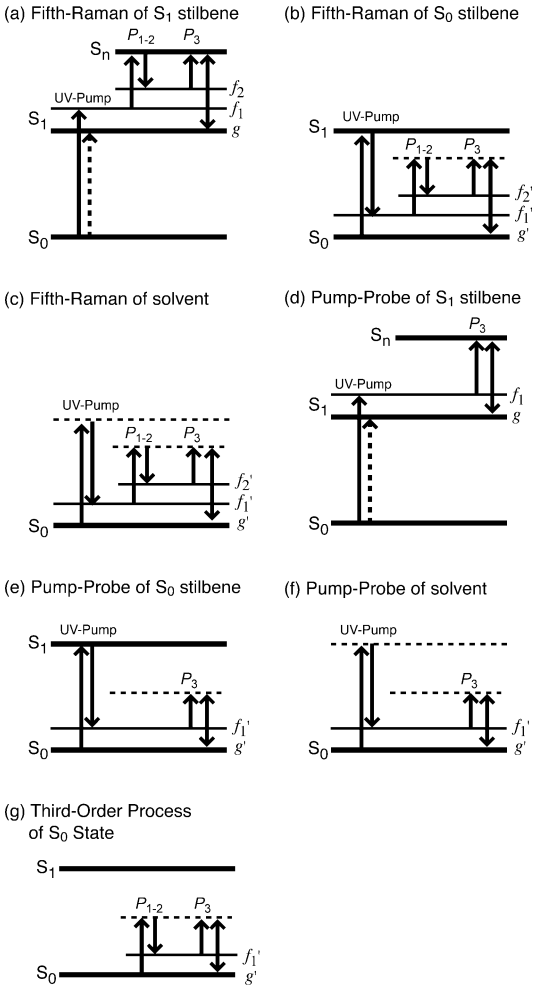

Figure 7. Energy diagrams of optical processes that irradiate light in the same direction as the fifth-order Raman signal: f'_1 and f'_2 are the vibrational excited states of the S_0 states of *trans*-stilbene or the solvent.

The absorbance change observed by the fifth-order Raman setup in Figure 3a is expressed by

$$\Delta A_{\text{obs}} = -\log(I_{\text{ON}}/I_{\text{OFF}}) \tag{4}$$

where I_{ON} and I_{OFF} represent the transmitted P_3 intensity with the P_{1-2} on and off, respectively. The intensity I_{ON} is

$$I_{\text{ON}} = |E_{\text{fifth}-S_1} + E_{\text{fifth}-S_0} + E_{\text{pump}-\text{probe}-S_1} + E_{\text{pump}-\text{probe}-S_0} + E_{\text{third}-S_0} + E_3|^2 \tag{5}$$

and I_{OFF} is

$$I_{\text{OFF}} = |E_{\text{pump}-\text{probe}-S_1} + E_{\text{pump}-\text{probe}-S_0} + E_3|^2 \tag{6}$$

where E_3 denotes the electric field of the input P_3 pulse. Assuming that the P_3 field (E_3) is much larger than the other fields, eq 4 is approximated as

$$\Delta A_{\text{obs}} \propto -E_{\text{fifth}-S_1}E_3^* - E_{\text{fifth}-S_0}E_3^* - E_{\text{third}-S_0}E_3^* \tag{7}$$

Figure 5 clearly shows that the oscillatory component in $E_{\text{third}-S_0}$ was negligible except for only the nonresonant electronic response around the time origin ($t_2 = 0$). In addition, the higher order field, $E_{\text{fifth}-S_0}$, is expected to be much smaller than the lower order field, $E_{\text{third}-S_0}$. Therefore, the oscillatory components in eq 7 are given by

$$\Delta A_{obs}^{OSC} \propto -E_{fifth-S_1}^{OSC} E_3^* \quad (8)$$

where ΔA_{obs}^{OSC} and $E_{fifth-S_1}^{OSC}$ denote the oscillatory component of ΔA_{obs} and $E_{fifth-S_1}$. The term of E_3 is independent of the delays of t_1 and t_2. Equation 8 indicates that the observed oscillatory component is linearly proportional to the fifth-order Raman field ($E_{fifth-S_1}^{OSC}$).

The 13 bands were presented on the FT spectra of $E_{fifth-S_1}^{OSC}$ (Figure 4). From the scheme of the fifth-order Raman spectroscopy (Figure 1a), the UV-pump pulse creates first vibrational coherence states of $|g\rangle\langle f_1|$ and $|f_1\rangle\langle g|$, as well as the population of the S_1 state ($|g\rangle\langle g|$ and $|f_1\rangle\langle f_1|$). The 13 bands can be attributed to $|g\rangle\langle f_1|$, $|f_1\rangle\langle g|$, $|g\rangle\langle g|$, and $|f_1\rangle\langle f_1|$. The lifetime of S_1 *trans*-stilbene in hexadecane ($|g\rangle\langle g|$, 119 ps)[35] and the vibrational cooling time in hexadecane of $|f_1\rangle\langle f_1|$ ($\sim$10 ps)[36,37] are much longer than the dephasing time of the vibrational coherence state of $|g\rangle\langle f_1|$ and $|f_1\rangle\langle g|$. For example, the dephasing time of $|g\rangle\langle \nu_{25}|$ and $|\nu_{25}\rangle\langle g|$ is 0.5 ps (Figure 3b). Thus, the short-lived bands at 193 and 398 cm^{-1} (Figure 4) are attributed to the first coherence states of $|g\rangle\langle f_1|$ and $|f_1\rangle\langle g|$. On the other hand, Figure 4a−d,f−j show that the 11 bands at 287, 461, 615, 721, 781, 843, 978, 1071, 1143, 1174, and 1234 cm^{-1} appeared at $t_1 =$ 2.000 ps. They mainly originated from the population of the S_1 state ($|g\rangle\langle g|$ and $|f_1\rangle\langle f_1|$). The frequency and bandwidth of the 11 bands agreed with those of the time-resolved spontaneous Raman bands of S_1 *trans*-stilbene.[24] Therefore, the 11 bands in the fifth-order Raman spectra are regarded as equivalents of the third-order Raman bands of S_1 *trans*-stilbene. Finally, we mention an additional contribution of the 11 bands at the early time delays of t_1. The intensities of these bands at the early time delays of t_1 were slightly different from those at $t_1 = 2.000$ ps (Figure 4). The difference might have originated from a contribution of the first coherence state of $|g\rangle\langle f_1|$ and $|f_1\rangle\langle g|$. When the first coherence states of $|g\rangle\langle f_1|$ and $|f_1\rangle\langle g|$ were transferred to the second coherence states of the eleven modes ($|g\rangle\langle f_2|$ and $|f_2\rangle\langle g|$) in the fifth-order Raman process (Figure 1a), the intensities of the bands in the FT spectra may have been different from those of the 11 bands appearing at $t_1 =$ 2.000 ps.

6. Summary

We performed a time-domain observation of the fifth-order Raman scattering of S_1 *trans*-stilbene in hexadecane. The FT spectrum contained 13 bands, and the band characteristics of two bands at 193 and 398 cm^{-1} were sensitive to t_1. The 193-cm^{-1} band was assigned to the P_{1-2} induced depletion process of the UV-induced vibrational coherence (ν_{25}). The depletion process of the UV-induced first coherence state and the stepwise creation of the coherence of the ν_{25} mode by UV-pump and the first visible (P_{1-2}) pulses may have contributed to the 398 cm^{-1}. The other 11 bands were equivalent to the time-resolved spontaneous Raman scattering. In the present work, we demonstrated the ability of fifth-order Raman spectroscopy to probe overtone and combination bands of excited-state molecules.

References and Notes

(1) Tanimura, Y.; Mukamel, S. *J. Chem. Phys.* **1993**, *99*, 9496.
(2) Okumura, K.; Tanimura, Y. *Chem. Phys. Lett.* **1997**, *278*, 175.
(3) Tominaga, K.; Yoshihara, K. *Phys. Rev. Lett.* **1995**, *74*, 3061.
(4) Tominaga, K.; Yoshihara, K. *Phys. Rev. Lett.* **1996**, *76*, 987.
(5) Steffin, T.; Duppen, K. *Phys. Rev. Lett.* **1996**, *76*, 1224.
(6) Tokmakoff, A.; Fleming, G. R. *J. Chem. Phys.* **1996**, *106*, 2569.
(7) Tokmakoff, A.; Lang, M. J.; Larsen, D. S.; Fleming, G. R.; Chernyak, V.; Mukamel, S. *Phys. Rev. Lett.* **1997**, *79*, 2702.
(8) Ivanecky, J. E.; Wright, J. C. *Chem. Phys. Lett.* **1993**, *206*, 437.
(9) Kirkwood, J. C.; Ulness, D. J.; Albrecht, A. C.; Stimson, M. J. *Chem. Phys. Lett.* **1998**, *293*, 417.
(10) Blank, D. A.; Kaufman, L. J.; Fleming, G. R. *J. Chem. Phys.* **1999**, *111*, 3105.
(11) Kano, H.; Hamaguchi, H. *J. Chem. Phys.* **2003**, *118*, 4556.
(12) Kubarych, K. J.; Miline, C. J.; Lin, S.; Astinov, V.; Miller, R. J. D. *J. Chem. Phys.* **2002**, *116*, 2016.
(13) Kaufman, L. J.; Heo, J.; Ziegler, L. D.; Fleming, G. R. *Phys. Rev. Lett.* **2002**, *88*, 207402.
(14) Takeuchi, S.; Tahara, T. *Chem. Phys. Lett.* **2000**, *326*, 430.
(15) Takeuchi, S.; Tahara, T. *J. Chem. Phys.* **2004**, *120*, 4768.
(16) Lochbrunner, S.; Wurzer, A. J.; Riedle, E. *J. Chem. Phys.* **2000**, *112*, 10699.
(17) Banin, U.; Ruhman, S. *J. Chem. Phys.* **1993**, *99*, 9318.
(18) Fujiyoshi, S.; Takeuchi, S.; Tahara, T. *J. Phys. Chem. A* **2003**, *107*, 494.
(19) Cerullo, G.; Lüer, L.; Manzoni, C.; Silvestri, S. D.; Shoshana, O.; Ruhman, S. *J. Phys. Chem. A* **2003**, *107*, 8339.
(20) Fujiyoshi, S.; Takeuchi, S.; Tahara, T. *J. Phys. Chem. A* **2004**, *108*, 5938.
(21) Anderson, N. A.; Durfee, C. G., III; Murnane, M. M.; Kapteyn, H. C.; Sension, R. J. *Chem. Phys. Lett.* **2000**, *323*, 365.
(22) Green, B. I.; Hochstrasser, R. M.; Weisman, R. B. *Chem. Phys. Lett.* **1979**, *62*, 427.
(23) Iwata, K.; Hamaguchi, H. *J. Phys. Chem. A* **1997**, *101*, 632.
(24) Gustafson, T. L.; Roberts, D. M.; Chernoff, D. A. *J. Chem. Phys.* **1984**, *81*, 3438.
(25) Syage, J. A.; Felker, P. M.; Zewail, A. H. *J. Chem. Phys.* **1984**, *81*, 4685.
(26) Urano, T.; Hamaguchi, H.; Tasumi, M.; Yamanouchi, K.; Tsuchiya, S.; Gustafson, T. L. *J. Chem. Phys.* **1989**, *91*, 3884.
(27) Watanabe, H.; Okamoto, Y.; Furuya, K.; Sakamoto, A.; Tasumi, M. *J. Phys. Chem. A* **2002**, *106*, 3318.
(28) Ziegler, L. D.; Fan, R.; Desrosiers, A. E.; Scherer, N. F. *J. Chem. Phys.* **1994**, *100*, 1823.
(29) Nagasawa, Y.; Watanabe, A.; Takikawa, H.; Okada, T. *J. Phys. Chem. A* **2003**, *107*, 632.
(30) Fujiyoshi, S.; Ishibashi, T.; Onishi, H. *J. Phys. Chem. B* **2004**, *108*, 1525.
(31) Fujiyoshi, S.; Ishibashi, T.; Onishi, H. *J. Phys. Chem. B* **2004**, *108*, 10636.
(32) In the nonresonant case, the band characteristics are opposite of those in the resonant case.[28,38−41] The FT spectra of the vibrational coherence in the nonresonant condition have symmetric shapes in the imaginary part and dispersive shapes in the real parts.
(33) Ruhman, S.; Willliams, L. R.; Joly, A. G.; Kohler, B.; Nelson, K. A. *J. Phys. Chem.* **1987**, *91*, 2237.
(34) Hamaguchi, H. *Chem. Phys. Lett.* **1986**, *126*, 185.
(35) Courtney, S. H.; Kim, S. K.; Canonica, S.; Fleming, G. R. *J. Chem. Soc., Faraday Trans. 2* **1986**, *82*, 2065.
(36) Sarkar, N.; Takeuchi, S.; Tahara, T. *J. Phys. Chem. A* **1999**, *103*, 4808.
(37) Schwarzer, D.; Troe, J.; Votsmeier, M.; Zerezke, M. *J. Chem. Phys.* **1996**, *105*, 3121.
(38) McMorrow, D.; Lotshaw, W. T. *J. Phys. Chem.* **1991**, *95*, 10395.
(39) Castner, E. W.; Chang, Y. J.; Chu, Y. C.; Walrafen, G. E. *J. Chem. Phys.* **1995**, *102*, 653.
(40) Vöhringer, P.; Scherer, N. F. *J. Phys. Chem.* **1995**, *99*, 2684.
(41) Matsuo, S.; Tahara, T. *Chem. Phys. Lett.* **1997**, *264*, 636.